Journal of Power Sources 267 (2014) 1–8

Contents lists available at ScienceDirect

Journal of Power Sources

journal homepage: www.elsevier.com/locate/jpowsour

An all-solid-state perovskite-sensitized solar cell based on the dual function polyaniline as the sensitizer and p-type hole-transporting material

Yaoming Xiao*, Gaoyi Han*, Yunzhen Chang, Haihan Zhou, Miaoyu Li, Yanping Li

Institute of Molecular Science, Key Laboratory of Chemical Biology and Molecular Engineering of Education Ministry, Shanxi University, Taiyuan 030006, PR China

HIGHLIGHTS

- Polyaniline with brachyplast structure was electropolymerized and characterized.
- The polyaniline acted as the sensitizer and p-type HTM for the ass-PSSC.
- The ass-PSSC delivered a photovoltaic conversion efficiency of 7.34%.
- The ass-PSSC demonstrated a good long-term stability after 1000 h.

GRAPHICAL ABSTRACT

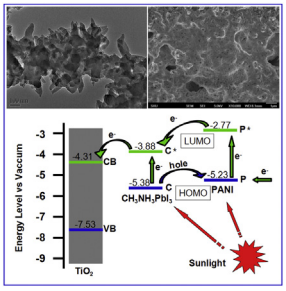

ARTICLE INFO

Article history:
Received 12 February 2014
Received in revised form
18 April 2014
Accepted 7 May 2014
Available online 21 May 2014

Keywords:
Polyaniline
Sensitizer
p-type hole-transporting material
All-solid-state perovskite-sensitized solar cell

ABSTRACT

High performance dual function of polyaniline (PANI) with brachyplast structure is synthesized by using a two-step cyclic voltammetry (CV) approach onto the fluorinated tin oxide (FTO) glass substrate, which acts as the sensitizer and p-type hole-transporting material (p-HTM) for the all-solid-state perovskite-sensitized solar cell (ass-PSSC) due to its $\pi-\pi^*$ transition and the localized polaron. The ass-PSSC based on the PANI delivers a photovoltaic conversion efficiency of 7.34%, and reduces from 7.34% to 6.71% after 1000 h, thereby 91.42% of the energy conversion efficiency is kept, indicating the device has a good long-term stability.

1. Introduction

Dye-sensitized solar cells (DSSCs) have attracted scientific and technological interest of researchers in the past decades as a high efficiency and low-cost alternative to conventional silicon p–n junction photovoltaic devices [1–3]. This kind of device based on a dye-sensitized porous nanocrystalline TiO_2 photoanode, an iodine-based liquid electrolyte, and a platinum counter electrode in a sandwich-like architecture, allowed an achievement of the efficiency of up to 12.3% [2]. Recently, a new class of hybrid organic-inorganic perovskite compounds ($CH_3NH_3PbX_3$, X = I, Br and Cl) replace the traditional dye (N719) as light harvesters for solar cells due to their direct band gap, wide light-absorption, and high carrier mobility [4–10]. The perovskite-sensitized solar cell (PSSC) presents an impressive high open circuit voltage and realizes an all-

* Corresponding authors. Tel.: +86 351 7010699; fax: +86 351 7016358.
E-mail addresses: ymxiao2011@sohu.com (Y. Xiao), han_gaoyis@sxu.edu.cn (G. Han).

http://dx.doi.org/10.1016/j.jpowsour.2014.05.053
0378-7753/

solid-state solar cell by replacing the liquid electrolyte with a hole transporting material (HTM) for the production and stability of the photovoltaic device [11,12].

The most commonly used HTM is 2,2′,7,7′-tetrakis-(N,N-di-p-methoxyphenylamine)-9,9′-spiro-biuorene (spiro-MeOTAD) [4–10], which demonstrates low recombination rate, efficient charge transport, and also good pore filling of the TiO_2 layer improving device performance. Of course, poly-triarylamine (PTAA) [5], poly(3-hexylthiophene) (P3HT) [13] are also used as the HTMs. However, Z. Ku et al. reported on carbon counter electrode in perovskite-based solar cells without HTMs, and achieved an efficiency of 6.64% [14]. For the sake of low cost, good stability, and simple easy preparation of designable structures, the p-type conducting polymers, e.g., polypyrrole (PPy) [15], polyaniline (PANI) [16,17], and poly(3,4-ethylenedioxythiophene) (PEDOT) [18–20] have been employed as cheaper alternatives in all-solid-state DSSCs. Among them, PANI has already been reported as a cost-effective and stable p-type HTM (p-HTM) and sensitizer in a solid-state DSSCs [16,17]. For instance, Tan et al. reported on the polyaniline as a hole transport material to prepare solid solar cells [16]. Senadeera et al. were successful at depositing PANI via molecular self-assembly on TiO_2 and using as a sensitizer in the solid-state solar cell [17].

It is well known that the PANI can be easily prepared through chemical polymerization [21] and electropolymerization methods [22–29]. The electropolymerization methods are considerably simpler and more cost-effective technique to obtain conducting polymers with the controllable surface morphology and well adhesion on the substrate surface. The reported electropolymerization methods used in synthesizing PANI include: the cyclic voltammetry (CV) [22,23], constant potential [24,25], constant current [26], pulse current [27], and pulse potentiostatic [28] methods. Recently, we investigated a two-step CV approach for the preparation of PANI, which quickly yielding high performance PANI with brachyplast structure [29].

Therefore, by considering these facts, here we report on an all-solid-state perovskite-sensitized solar cell (ass-PSSC) based on the PANI with brachyplast structure as the p-HTM, which was quickly electropolymerized by using the two-step CV method onto the fluorinated tin oxide (FTO) glass substrates. In addition, the PANI also acted as a function of sensitizer enhancing the device performance. Thus the ass-PSSC assembled with the PANI electrode exhibited a superior photovoltaic conversion of 7.34%, and showing a good long-term stability.

2. Experimental

2.1. Materials

Aniline monomer, sulfuric acid, acetone, isopropyl alcohol, methanol, ether, hydroiodic acid (45 wt.% in water), methylamine (30% in methanol), lead iodide (PbI_2), chlorobenzene, acetonitrile, tetrabutyl titanate, and Triton X-100 were purchased from Shanghai Chemical Agent Ltd., China (Analysis purity grade). γ-butyrolactone (>99.9%), tetrabutylammonium hexafluorophosphate ($TBAPF_6$, 98%), and ferrocene (>99.9%) were purchased from Aladdin. 4-tert-butyl-pyridine (TBP), lithium iodide (LiI), and lithium bis(trifluoromethylsulphonyl) imide (Li-TFSI) were purchased from Aldrich. The above agents were used without further purification.

2.2. PANI electrodes electropolymerization

The two-step CV electropolymerization of PANI [29] was carried out using a computer-controlled Autolab potentiostat (Type III) at ambient atmosphere. In brief, the potential range was firstly set between −0.1 V and 1.2 V for 1 cycle for the pre-electro- polymerization and then subjected to the second-step for the PANI electropolymerization between −0.1 V and 0.7 V for 10 cycles vs. Ag/AgCl at a scan rate of 0.025 V s^{-1} (shown in Fig. S1). Prior to electropolymerization, FTO substrates (1.5 cm × 2 cm) were cleaned with acetone and isopropyl alcohol, respectively. A Pt wire, a saturated silver/silver chloride (Ag/AgCl), and a cleaned FTO glass substrate were used as the counter electrode, the reference electrode, and the working electrode, respectively. All the PANI electrodes were electropolymerized on the FTO glass substrates (NSG, 8 Ω sq^{-1}) from an aqueous solution containing 0.5 M aniline monomer and 0.5 M sulfuric acid in a three compartment cell. The achieved PANI electrode was rinsed in distilled water and dried under a cool air flow.

2.3. Perovskite sensitizer synthesis

The perovskite sensitizer $CH_3NH_3PbI_3$/γ-butyrolactone solution was synthesized according to the reported procedure [5]. The CH_3NH_3I was prepared by reacting 20 mL hydroiodic acid (45 wt.% in water) and 20 mL methylamine (30% in methanol) in a 250 mL round-bottomed flask at 0 °C for 2 h with stirring. Then the resulting solution was evaporated at 50 °C for 1 h. The precipitate was washed three times with diethyl ether, dried at 60 °C under a vacuum oven for 24 h, and used without further purification. The synthesized CH_3NH_3I powder (0.395 g) was mixed with PbI_2 (1.157 g) in γ-butyrolactone (2 mL) at 60 °C for 12 h with stirring, finally, the perovskite sensitizer $CH_3NH_3PbI_3$/γ-butyrolactone solution was obtained. X-ray diffraction pattern of the $CH_3NH_3PbI_3$ was shown in Fig. S2. Strong diffraction peaks are observed at approximately 14.11, 19.99, 23.49, 24.48, 28.44, 31.88, 34.97, 40.44, and 43.04°, respectively corresponding to the reflections from (110), (112), (211), (202), (220), (310), (312), (224), and (314) crystal planes of the tetragonal perovskite structure [30].

2.4. TiO_2 photoanodes preparation

A layer of dense blocking TiO_2 (bl-TiO_2) was coated onto a FTO substrate by spin-coating of 30 mM tetrabutyl titanate in isopropyl alcohol with a small quantity of Triton X-100 at 500 r.p.m. for 15 s then at 6000 r.p.m. for 30 s, then heat-treated at 450 °C for 30 min. The mesoporous TiO_2 (mp-TiO_2) film was spin-coated on the bl-TiO_2 substrate under the same coating parameters using the TiO_2 colloid, which was prepared according to our previous reports [31,32]. The film was calcined again at 450 °C for 30 min, thereby the TiO_2 photoanode was gained.

2.5. Solar cell fabrication

The ass-PSSC-A was assembled by using the respectively as-prepared PANI electrode and TiO_2 photoanode in a sandwich-like architecture (shown in Fig. S3). Then the perovskite sensitizer $CH_3NH_3PbI_3$/γ-butyrolactone solution was injected into the ass-PSSC-A by using an injector, and dried in a vacuum oven at 80 °C for 12 h to obtain the solar cell, which was described as the ass-PSSC-B. In addition, a Li-salt solution composed of 0.032 M Li-TFSI, 0.032 M LiI, and 0.2 M TBP in the mixed solvent of chlorobenzene and acetonitrile (chlorobenzene : acetonitrile = 1:0.1 v/v), was further employed as an additive into the ass-PSSC-B to enhance the transporting ability for the electron and hole, and dried in a vacuum oven at 60 °C for 4 h, finally acquiring the device of ass-PSSC-C. The PANI electrodes and TiO_2 photoanodes based on the ass-PSSC-A, ass-PSSC-B, and ass-PSSC-C were described as the PANI, PANI-$CH_3NH_3PbI_3$, PANI-$CH_3NH_3PbI_3$–Li-salt electrodes and

TiO_2, TiO_2–$CH_3NH_3PbI_3$, TiO_2–$CH_3NH_3PbI_3$–Li-salt photoanodes, respectively.

2.6. Characterizations and measurements

The surface morphologies of the PANI electrodes and TiO_2 photoanodes were observed using a scanning electron microscopy (SEM, JEOL-JSM-6701F) operating at 10 kV. Transmission electron microscope (TEM, JEOL-JSM-2100) for the structure feature of the PANI was operated at 200 kV. Fourier transform infrared spectra (FTIR) of samples were recorded on an Infrared Spectrometric Analyzer (BRUKER TENSOR 27) using KBr as pellets. The phase identification of the $CH_3NH_3PbI_3$ was conducted with powder X-ray diffraction (XRD, BRUKER D8-ADVANCE), by which the $CH_3NH_3PbI_3$ powder was compacted on the plastic substrate attached to the XRD, and the powder was obtained by drying the $CH_3NH_3PbI_3$/γ-butyrolactone solution and following a grinding process. Ultraviolet to visible (UV–Vis) absorbance spectra of the samples were performed with an Agilent 8453 UV–Vis diode array spectrophotometer. Cyclic voltammetry was carried out on a computer-controlled Autolab potentiostat (Type III) in a solution of tetrabutylammonium hexafluorophosphate ($TBAPF_6$) (0.1 M) in anhydrous acetonitrile at a scan rate of 100 mV s at room temperature under argon protection. A FTO glass electrode was used as the working electrode (WE), each materials were deposited on the WE. A platinum wire was used as the counter electrode. As a reference electrode (RE), a silver wire coated with AgCl was used. After each measurement, the RE was calibrated with ferrocene.

The electrochemical impedance spectroscopy (EIS) of the ass-PSSC was performed using a CHI660D (Shanghai Chenhua Device Company, China) electrochemical measurement system at a constant temperature of 20 °C in ambient atmosphere under illumination by a solar simulator (CEL-S500, Beijing Ceaulight Science and Technology Ltd., China), and the impedance data covered a frequency range of 1–10^5 Hz with 5 mV of amplitude and zero bias potential. The resultant impedance spectra were simulated using the Z-view software. The incident monochromatic photon-to-current conversion efficiency (IPCE) curves were measured with a solar cell QE/IPCE measurement system (Solar Cell Scan 100, Beijing Zolix Instruments Co. Ltd., China). The photocurrent density–voltage (J–V) characteristic of the ass-PSSC was carried out using a computer-controlled CHI660D in ambient atmosphere. The incident light intensity was set under 100 mW cm^{-2} (AM1.5), and a black mask (0.50 cm^2) was used on top of the device to control the active cell area for the light irradiation. The photoelectronic performances [i. e., fill factor (*FF*) and overall energy conversion efficiency (η)] were calculated by the following equations [33]:

$$FF = \frac{V_{max} \times J_{max}}{V_{oc} \times J_{sc}} \tag{1}$$

$$\eta(\%) = \frac{V_{max} \times J_{max}}{P_{in}} \times 100\% = \frac{V_{oc} \times J_{sc} \times FF}{P_{in}} \times 100\% \tag{2}$$

where J_{SC} is the short-circuit current density (mA cm^{-2}), V_{OC} is the open-circuit voltage (V), P_{in} is the incident light power, J_{max} (mA cm^{-2}) and V_{max} (V) are the current density and voltage in the J–V curves at the point of maximum power output, respectively.

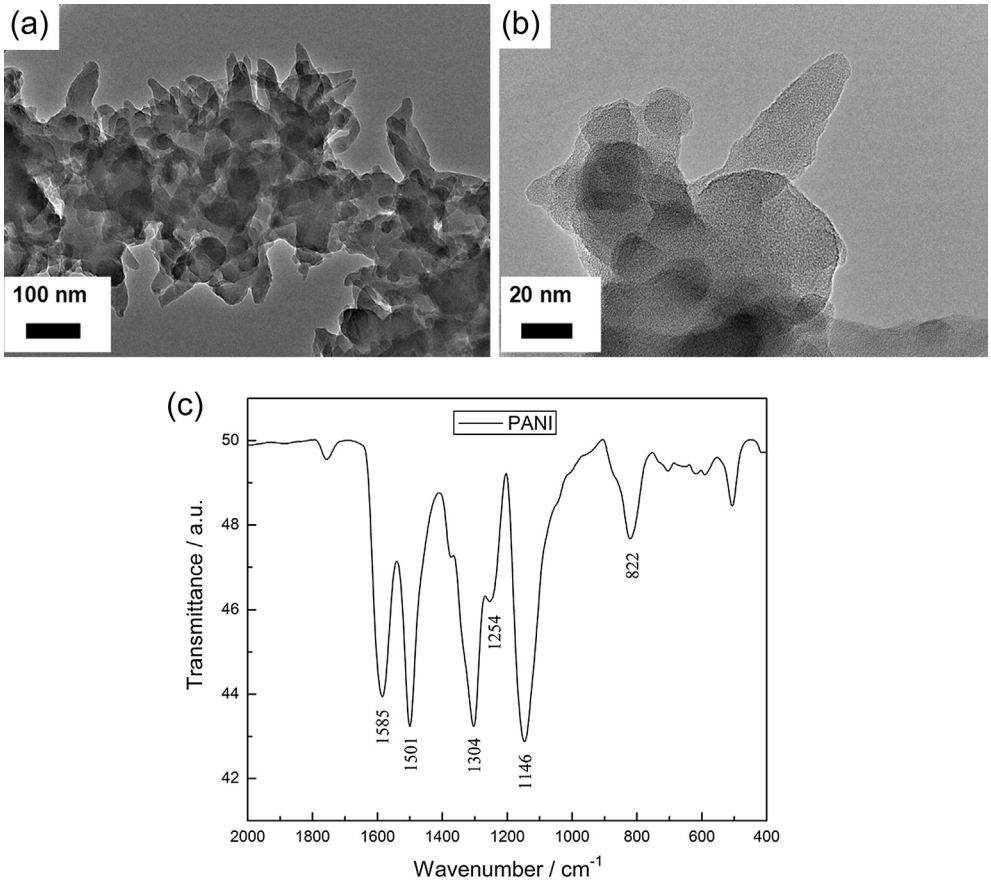

Fig. 1. (a and b) TEM images and (c) FTIR spectrum of the two-step CV PANI.

3. Results and discussion

3.1. Structure feature and composition of the PANI

Fig. 1(a and b) (higher magnification) show TEM images to investigate the structure feature of the PANI. It can be found that the PANI with brachyplast structure could be obtained on the FTO substrate by using the two-step CV approach, this structure likes that some tiny twigs germinate on the tree branch. The brachyplast PANIs with the diameter of 15–30 nm and the length of 30–60 nm was electropolymerized on the pre-electropolymerized PANIs, which has been confirmed that the nanoscale brachyplast PANIs can increase the active surface area in our previous report [29], thus being expected to enhance the light absorbance and contact with the perovskite sensitizer $CH_3NH_3PbI_3$.

To characterize the composition of the electropolymered PANI, the PANI was collected together from the FTO glass, and the FTIR spectrum of the PANI was performed. As shown in Fig. 1(c), the characteristic peaks at 1585 and 1501 cm^{-1} belong to the C=C stretching of quinoid ring and benzenoid deformation of the PANI, respectively. The bands at 1304 and 1254 cm^{-1} are attributed to benzenoid ring C–N stretching mode and bending mode, respectively. The contribution from C–H bending of the quinoid ring appears at 1146 cm^{-1}. The absorption band at 822 cm^{-1} belongs to the out-of-plane bending vibration of C–H on the 1,4-disubstituted ring [28,29,34,35]. The FTIR spectrum indicates that the PANI was successfully deposited onto the surfaces of FTO glass substrates.

3.2. Morphology of the PANI electrode

The SEM images of the PANI, PANI-$CH_3NH_3PbI_3$, and PANI-$CH_3NH_3PbI_3$–Li-salt electrodes are shown in Fig. 2. It can be found that the PANI electrode with uniform and porous morphology was generated on the FTO substrate (Fig. 2(a)). It should be noticed that the electropolymerization time was sharply cut down by using the two-step CV approach compared to the one-step CV mode [29]. After injecting the perovskite sensitizer $CH_3NH_3PbI_3$, the porous PANI film was filled with $CH_3NH_3PbI_3$ (Fig. 2(b)). Moreover, the Li-salt was applied to fill in most holes to connect $CH_3NH_3PbI_3$ perovskite nanoparticles and enhance the contact between the PNAI electrode and TiO_2 anode (Fig. 2(c)). Fig. 2(d) shows the cross-sectional SEM image of the PANI-$CH_3NH_3PbI_3$–Li-salt electrode, the thickness of the PANI film is about 1.8 μm, and the PANI film with three-dimensional space was well combined on the FTO substrate. A similar dynamic can be seen in the TiO_2, TiO_2–$CH_3NH_3PbI_3$, and TiO_2–$CH_3NH_3PbI_3$–Li-salt photoanodes (Fig. S4). $CH_3NH_3PbI_3$ and Li-salt were well deposited on the TiO_2 anode with a thickness of 1.8 μm, and on which the thickness of the TiO_2 film was about 0.2 μm (Fig. S4d). The $CH_3NH_3PbI_3$ film has a diffusion length of 129 ± 41 nm for electrons and 105 ± 35 nm for holes [10], which requests that the thickness of the PANI and TiO_2 films should be thinner than the diffusion length, respectively. For this consideration, the introduction of the Li-salt would enhance the transporting ability for the electron and hole in the $CH_3NH_3PbI_3$ perovskite nanoparticles between the PNAI electrode and TiO_2 anode, which would reduce the demand of the thickness of the PANI and TiO_2 films, further influence the performance of the ass-PSSC especially the fill factor.

3.3. Optical and electrochemical properties of the PANI electrode

Fig. 3 compares the UV–Vis absorption spectra of the PANI electrode, pure $CH_3NH_3PbI_3$ film, and PANI-$CH_3NH_3PbI_3$ electrode, respectively, they are all prepared on the FTO glass substrates. The hump at 350 nm is observed for pristine PANI, which is assigned to π–π^* transition centered on the benzenoid rings, and the peak at

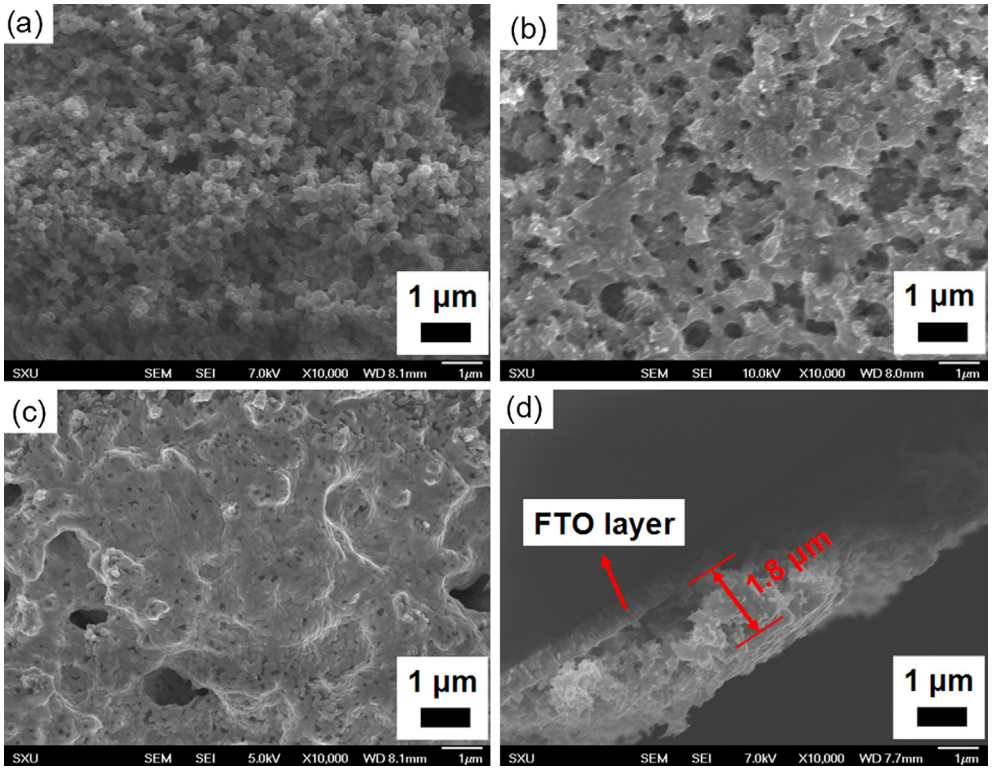

Fig. 2. SEM images of the (a) PANI, (b) PANI-$CH_3NH_3PbI_3$, and (c) PANI-$CH_3NH_3PbI_3$–Li-salt electrodes, respectively; (d) Cross-sectional SEM image of the PANI-$CH_3NH_3PbI_3$–Li-salt electrode.

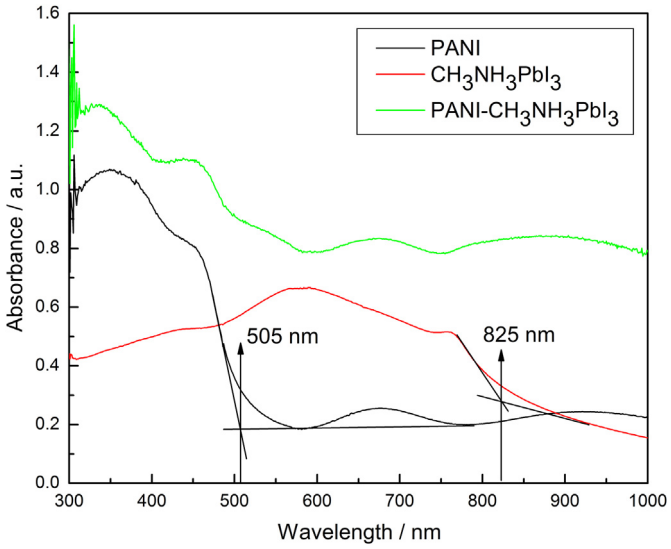

Fig. 3. UV–Vis absorption spectra of the PANI, $CH_3NH_3PbI_3$, and PANI-$CH_3NH_3PbI_3$ electrodes, respectively.

450 nm corresponds to the localized polarons caused by the interband charge transfer from benzenoid to quinoid moieties of the PANI [36,37]. The $CH_3NH_3PbI_3$ film has a broad absorption at around 400–800 nm and absorbs strongly below 580 nm [8,30,38]. Additionally, the curve of the PANI-$CH_3NH_3PbI_3$ exhibits superposed absorption characteristics of the PANI and $CH_3NH_3PbI_3$ film. The broad absorption window overlapping with the maximum irradiance of the solar spectrum ensures efficient photon harvesting, which may eventually lead to a high photocurrent. A similar dynamic can be found in the TiO_2 photoanode, pure $CH_3NH_3PbI_3$ film, and TiO_2–$CH_3NH_3PbI_3$ photoanode (Fig. S5). While the TiO_2 has a strong absorption at the 320 nm replacing that of the PANI at 350 and 450 nm [8,30,38]. The optical band gap energy (E_g) of each material was calculated by using the equation of $E_g = 1240/\lambda$, in which the λ value was measured by UV–Vis absorption spectra (Fig. 3 and Fig. S5). The E_g values were listed in Table S1. PANI has a forbidden band gap of 2.46 eV. E_g for the $CH_3NH_3PbI_3$ deposited on TiO_2 film is demonstrated to be 1.50 eV, which presents that the optical absorption in the perovskite sensitizer occurs via a direct transition [39,40]. The E_g of the bare TiO_2 film is determined to be 3.22 eV, which is consistent with data reported elsewhere [39,40].

The electrochemical properties of each materials were studied by the cyclic voltammetry (CV), and the results were shown in Fig. S6. The highest occupied molecular orbital (HOMO) and the lowest unoccupied molecular orbital (LUMO) levels were estimated from the oxidation potential (E_{ox}) according to the empirical formulas of HOMO $= -(E_{ox} + 4.80 - E_{ox}(\text{Ferrocene}))$ and LUMO = HOMO + E_g, and the results were listed in Table S1. According to the results, Fig. 4 shows the schematic energy level diagram of the TiO_2, $CH_3NH_3PbI_3$, and PANI, respectively, where the band positions are well aligned for the charge separation. In the ass-PSSC, both the perovskite $CH_3NH_3PbI_3$ and PANI absorb the photons at their interface under sunlight, then charge separation occurs at the interface. Due to the well matched band positions for the charge separation, the photon-generated electrons from the excited perovskite $CH_3NH_3PbI_3$ (C*) and PANI (P*) can be quickly transferred to the conductive band (CB) of semiconductor TiO_2, and forming the photo-current by the external circuit.

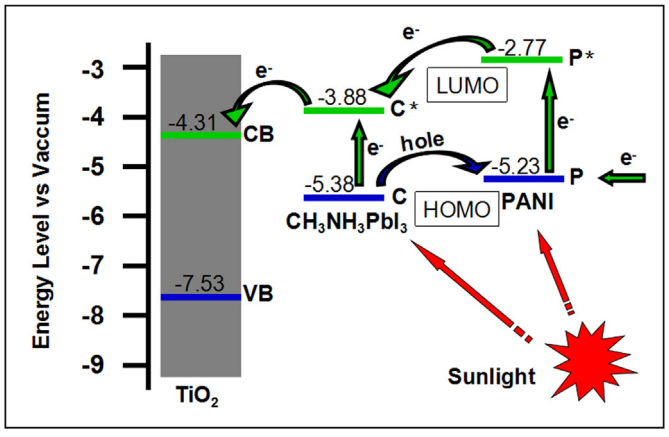

Fig. 4. Schematic energy level diagram of the TiO_2, $CH_3NH_3PbI_3$, and PANI.

Electrochemical impedance spectroscopy (EIS) was used to characterize the internal resistance and charge transfer kinetics of the solar cell [41,42], as shown in Fig. 5. The equivalent circuit of this model (Fig. S7) has been already reported [43–45]. The intercept of the real axis at high frequency is the ohmic series resistance (R_S) including the sheet resistance of the TiO_2 photoanode, the PANI electrode, and the $CH_3NH_3PbI_3$ resistance. The first semicircle at high frequency refers to the $R_{CT}(PANI)$ for the charge-transfer resistance at the PANI/$CH_3NH_3PbI_3$ interface, while the second semicircle at middle frequency refers to the $R_{CT}(TiO_2)$ for the charge-transfer resistance at the $CH_3NH_3PbI_3$/TiO_2 interface [43–45]. The constant phase elements (Y_{CPE}(PANI) and $Y_{CPE}(TiO_2)$) are frequently used as substitutes for the capacitors in an equivalent circuit to fit the impedance behavior of the electrical double layer more accurately while the double layer does not behave as an ideal capacitor [43–45].

The results of the impedance data are shown in Table 1. It can be seen that the R_S, R_{CT}(PANI), and $R_{CT}(TiO_2)$ values are gradually reduced by injecting the $CH_3NH_3PbI_3$ and Li-salt into the device, owing to the high carrier mobility of the $CH_3NH_3PbI_3$ and Li-salt were filled up in both the TiO_2 and PANI films. The R_S, R_{CT}(PANI), and $R_{CT}(TiO_2)$ values of the ass-PSSC-C are 8.82, 3.37, and 5.25 Ω cm^2, respectively, which are the lowest values among the three kinds of devices. The lower resistances could result in a more effective and rapid transporting ability for the electron and hole, which would further improve the performance of the ass-PSSC especially the fill factor. Based on the EIS model, the effective electron lifetime for recombination (τ_r) in the photoanode can be calculated from the minimum angular frequency (ω_{min}) value by the following equation: $\tau_r = 1/\omega_{min}$, where the ω_{min} values come from the impedance semicircle at middle frequencies in the Bode spectrum. The τ_r value for the device of ass-PSSC-A has a highest value of 47.10 ms, this is due to the lowest carrier mobility in the PANI electrode and TiO_2 photoanode. While the τ_r values for the ass-PSSCs-B and ass-PSSC-C have a same value of 14.34 ms, this may be owing to the high carrier mobility of the $CH_3NH_3PbI_3$ in the TiO_2 and PANI films for the reduced effective electron lifetime, but the Li-salt has little effect on the lifetime. The lower τ_r value could increase the electron recombination, resulting in a depressed cell performance [19,20,46]. However, the photon-generated electrons from the excited perovskite $CH_3NH_3PbI_3$ (C*) and PANI (P*) can be quickly separated and transferred to the conductive band (CB) of semiconductor TiO_2 in the level of femtosecond, therefore the 14.34 ms can provide enough time for the carrier transport [47].

3.4. Photovoltaic performance of the ass-PSSC

IPCEs of the three kinds of ass-PSSCs were characterized and are shown in Fig. 6(a), which reflects the light response of the PSSC and is directly related to the J_{SC}. It is noticeable that the IPCE curve for

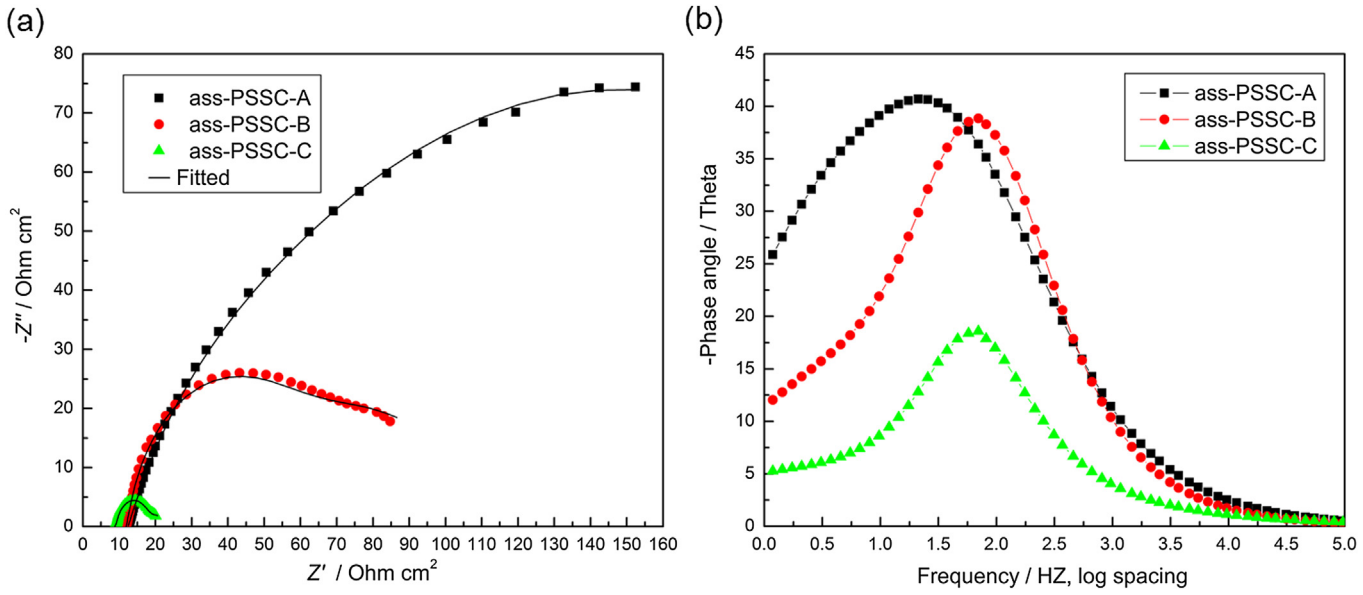

Fig. 5. (a) Nyquist plots and (b) Bode phase plots of the ass-PSSC-A, ass-PSSC-B, and ass-PSSC-C, respectively.

Table 1
EIS results of the ass-PSSC-A, ass-PSSC-B, and ass-PSSC-C, respectively.

Sample	R_S (Ω cm^2)	R_{CT}(PANI) (Ω cm^2)	R_{CT}(TiO_2) (Ω cm^2)	Y_{CPE}(PANI) (mF cm^{-2})	Y_{CPE}(TiO_2) (mF cm^{-2})	ω_{min} (Hz)	τ_r (ms)
ass-PSSC-A	12.50	8.89	125.65	0.93	0.68	21.23	47.10
ass-PSSC-B	11.96	7.49	30.64	0.87	0.65	69.75	14.34
ass-PSSC-C	8.82	3.37	5.25	0.84	0.61	69.75	14.34

the ass-PSSC-A has a photocurrent response from 350 nm to 450 nm, which is due to the π–π* transition and the localized polarons from the PANI [36,37], indicating the PANI can be used as a sensitizer in solar cells. After the introduction of $CH_3NH_3PbI_3$, the ass-PSSC-B shows a wide light response from 350 nm to higher than 750 nm, with the maximum at ca. 525 nm. Moreover, the Li-salt can observably reduce the internal resistances of the solar cell, then further enhance the IPCE performance of the ass-PSSC-C. These results were in agreement with the UV–Vis absorption spectra, EIS tests, and following *J*–*V* measurements.

The photovoltaic properties of ass-PSSCs were measured under full sunlight illumination (100 mW cm^{-2}, AM1.5 G), which were reproduced many times without obvious change, and the results were summarized in Table 2. As can be seen in Fig. 6(b), the ass-

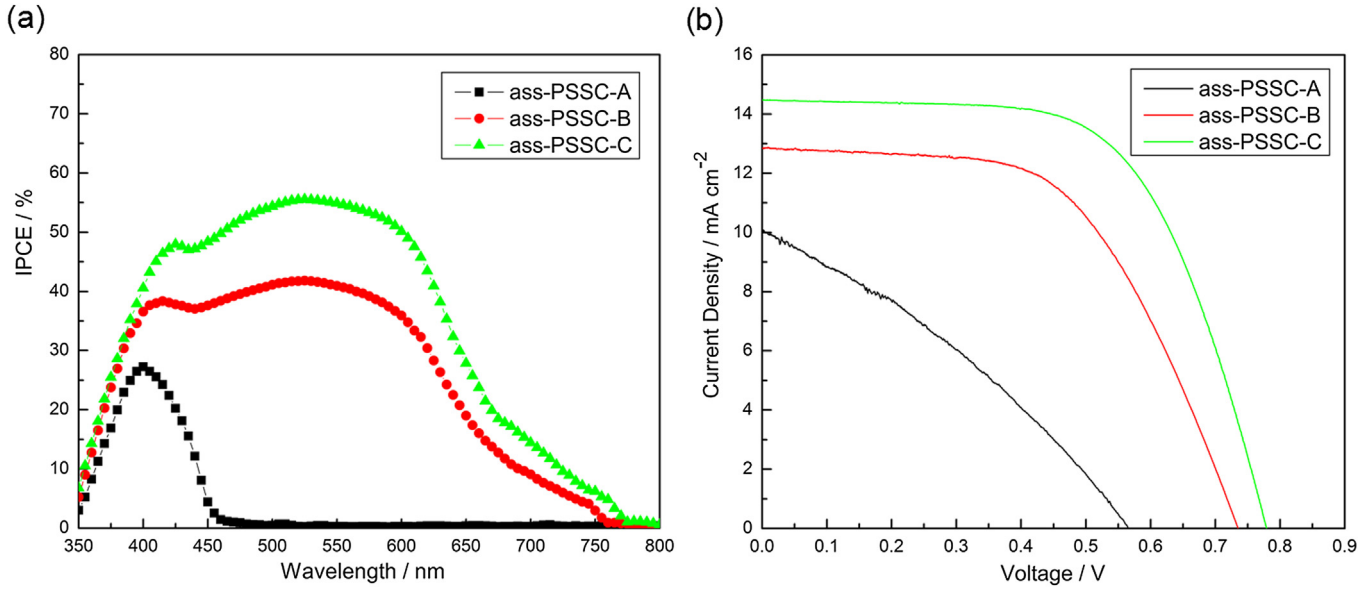

Fig. 6. (a) IPCE and (b) Photocurrent density–voltage characteristics of the ass-PSSC-A, ass-PSSC-B, and ass-PSSC-C, respectively.

Table 2
The photovoltaic performance of the ass-PSSC-A, ass-PSSC-B, and ass-PSSC-C, respectively.

Sample	J_{SC} (mA cm^{-2})	V_{OC} (V)	*FF*	η (%)
ass-PSSC-A	10.06 ± 0.04	0.57 ± 0.02	0.36 ± 0.02	2.06 ± 0.03
ass-PSSC-B	12.84 ± 0.05	0.74 ± 0.03	0.54 ± 0.02	5.13 ± 0.04
ass-PSSC-C	14.48 ± 0.06	0.78 ± 0.03	0.65 ± 0.03	7.34 ± 0.06

PSSC-A without $CH_3NH_3PbI_3$ and Li-salt produces a cell efficiency of 2.06%, proving the PANI with brachyplast structure has an absorption in the region of visible light, which can be used as a sensitizer in solar cells. And in this device, the energy levels between the PANI and the TiO_2 could be matched well to form a p–n junction for the charge separation [17]. However, the low efficiency of the ass-PSSC-A might be attributed to the partial absorption of visible light in the PANI film (shown in Fig. 3) and high electrochemical resistances between the PANI electrode and TiO_2 photoanode (shown in Fig. 5). To improve the photovoltaic performance of the device, adding a sensitizer of $CH_3NH_3PbI_3$ to broaden absorption of visible light and introducing the Li-salt to reduce the internal resistances of the solar cell, were carried out. As can be found in Fig. 6(b), the short-circuit current density (J_{SC}), open-circuit voltage (V_{OC}), and fill factor (*FF*) values of the ass-PSSC-B are observably increased by introducing the perovskite sensitizer into the solar cell. This is because of the TiO_2 and PANI films were filled up with broad absorption and high carrier mobility of the $CH_3NH_3PbI_3$. The fill factor (*FF*) value of the ass-PSSC-C is further enhanced by employing the Li-salt, attributing to the decreased values of the R_S, R_{CT}(PANI), and R_{CT}(TiO_2) [48,49]. As a result, the ass-PSSC-C demonstrates an acceptable *FF* value of 0.65, and supplies a cell efficiency of 7.34%.

Finally, the operational stability of the ass-PSSC-C was tested under light intensity of 100 mW cm^{-2} and shown in Fig. 7. As a whole, the photovoltaic performances and normalized efficiency decrease slightly with the continuation of time. However, the efficiency (η) of the device reduces from 7.34% to 6.71% after 1000 h, thereby 91.42% of the energy conversion efficiency is remained, indicating the device has a superior long-term stability.

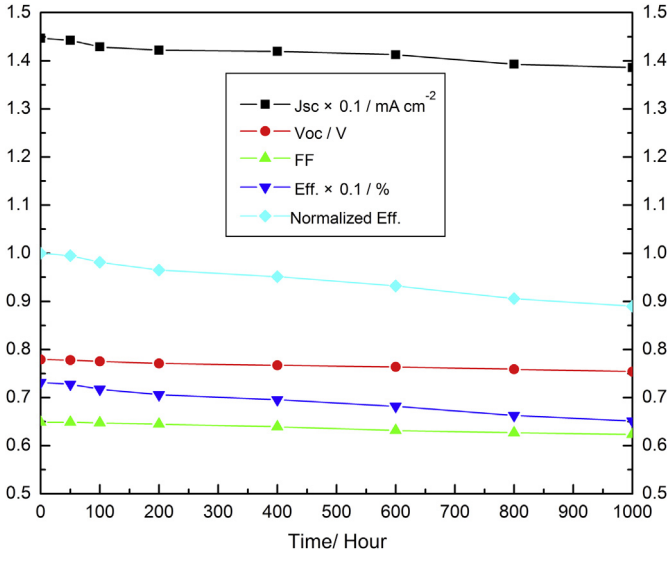

Fig. 7. Time-course changes of the normalized efficiency and photovoltaic performances of the ass-PSSC-C, under light intensity of 100 mW cm^{-2}.

4. Conclusions

In summary, dual function of PANI with brachyplast surface morphology was quickly electropolymerized by means of using a two-step CV approach, which acted as the sensitizer and p-HTM in ass-PSSCs. The PANI with the nanoscale brachyplast structure offered high active surface area for the light absorbance and efficient charge transport due to its π–π^* transition and the localized polaron. Furthermore, the porous PANI film could be filled up with $CH_3NH_3PbI_3$ and Li-salt, resulting in a wide light harvesting and an excellent carrier mobility, where the band positions were well aligned for charge separation. The low-cost ass-PSSC using the PANI yielded a conversion efficiency of 7.34% under full sunlight illumination (100 mW cm^{-2}, AM1.5 G), and reduced from 7.34% to 6.71% after 1000 h, thereby 91.42% of the energy conversion efficiency was kept, indicating the device had a good long-term stability. The present work suggests that the PANI shows a great potential as a cost-effective p-HTM for ass-PSSCs.

Acknowledgments

The authors appreciate funding from National Natural Science Foundation of China (21274082 and 21073115) and Shanxi Province (2012021021-3), the Program for New Century Excellent Talents in University (NCET-10-0926), and the Scientific Research Start-up Funds of Shanxi University (020351801003).

Appendix A. Supplementary data

Supplementary data related to this article can be found at http://dx.doi.org/10.1016/j.jpowsour.2014.05.053.

References

[1] B. O' Regan, M. Grätzel, Nature 353 (1991) 737.
[2] A. Yella, H. Lee, H. Tsao, C. Yi, A. Chandiran, M. Nazeeruddin, E. Diau, C. Yeh, S. Zakeeruddin, M. Grätzel, Science 334 (2011) 629.
[3] L. Han, As Islam, H. Chen, C. Malapaka, B. Chiranjeevi, S. Zhang, X. Yang, M. Yanagida, Energy Environ. Sci. 5 (2012) 6057.
[4] J. Burschka, N. Pellet, S. Moon, R. Humphry-Baker, P. Gao, M. Nazeeruddin, M. Grätzel, Nature 499 (2013) 316.
[5] J. Heo, S. Im, J. Noh, T. Mandal, C. Lim, J. Chang, Y. Lee, H. Kim, A. Sarkar, M. Nazeeruddin, M. Grätzel, S. Seok, Nat. Phot. 7 (2013) 486.
[6] J. Ball, M. Lee, A. Hey, H. Snaith, Energy Environ. Sci. 6 (2013) 1739.
[7] M. Liu, M. Johnston, H. Snaith, Nature 501 (2013) 395.
[8] M. Lee, J. Teuscher, T. Miyasaka, T. Murakami, H. Snaith, Science 338 (2012) 643.
[9] H. Kim, I. Mora-Sero, V. Gonzalez-Pedro, F. Fabregat-Santiago, E. Juarez-Perez, N. Park, J. Bisquert, Nat. Commun. 4 (2013) 2242.
[10] S.D. Stranks, G.E. Eperon, G. Grancini, C. Menelaou, M.J.P. Alcocer, T. Leijtens, L.M. Herz, A. Petrozza, H.J. Snaith, Science 342 (2013) 341.
[11] E. Edri, S. Kirmayer, D. Cahen, G. Hodes, J. Chem. Phys. Lett. 4 (2013) 897.
[12] J. Qiu, Y. Qiu, K. Yan, M. Zhong, C. Mu, H. Yan, S. Yang, Nanoscale 5 (2013) 3245.
[13] F. Giacomo, S. Razza, F. Matteocci, A. D'Epifanio, S. Licoccia, T. Brown, A. Carlo, J. Power Sources 251 (2014) 152.
[14] Z. Ku, Y. Rong, M. Xu, T. Liu, H. Han, Sci. Rep. 3 (2013) 3132.
[15] Y. Guo, Y. Zhang, H. Liu, S. Lai, Y. Li, Y. Li, W. Hu, S. Wang, C. Che, D. Zhu, J. Phys. Chem. Lett. 1 (2010) 327.
[16] S. Tan, J. Zhai, M. Wan, L. Jiang, D. Zhu, Synth. Met. 137 (2003) 1511.
[17] G. Senadeera, T. Kitamura, Y. Wada, S. Yanagida, J. Photochem. Photobiol. A 164 (2004) 61.
[18] J. Xia, N. Masaki, N. Lira-Cantu, Y. Kim, K. Jiang, S. Yanagida, J. Am. Chem. Soc. 130 (2008) 1258.
[19] J. Kim, J. Koh, B. Kim, S. Ahn, H. Ahn, D. Ryu, J. Kim, E. Kim, Adv. Funct. Mater. 21 (2011) 4633.
[20] J. Koh, J. Kim, B. Kim, J. Kim, E. Kim, Adv. Mater. 23 (2011) 1641.
[21] Q. Li, J. Wu, Q. Tang, Z. Lan, P. Li, J. Lin, Electrochem. Commun. 10 (2008) 1299.
[22] X. Zhao, J. Zang, Y. Zang, Y. Wang, L. Bian, J. Yu, Electrochem. Commun. 11 (2009) 1297.
[23] J. Zhang, T. Hreid, X. Li, W. Guo, L. Wang, X. Shi, H. Su, Z. Yuan, Electrochim. Acta 55 (2010) 3664.
[24] L. Hung, Z. Wang, H. Wang, X. Cheng, A. Mitra, Y. Yan, J. Mater. Chem. 12 (2002) 388.

[25] K. Huang, J. Huang, C. Wu, C. Liu, H. Chen, C. Chu, J. Lin, C. Lin, K. Ho, J. Mater. Chem. 21 (2011) 10384.
[26] Z. Li, B. Ye, X. Hu, X. Hu, X. Ma, X. Zhang, Y. Deng, Electrochem. Comm. 11 (2009) 1768.
[27] H. Karami, M.G. Asadi, M. Mansoori, Electrochim. Acta 61 (2012) 154.
[28] Y. Xiao, J. Lin, J. Wu, S. Tai, G. Yue, J. Power Sources 233 (2013) 320.
[29] Y. Xiao, G. Han, Y. Li, M. Li, Y. Chang, J. Mater. Chem. A 2 (2014) 3452.
[30] Y. Zhao, K. Zhu, J. Phys. Chem. Lett. 4 (2013) 2880.
[31] J. Wu, Z. Lan, J.M. Lin, M. Huang, S. Hao, T. Sato, S. Yin, Adv. Mater. 19 (2007) 4006.
[32] J. Wu, Y. Xiao, G. Yue, Q. Tang, J. Lin, M. Huang, Y. Huang, L. Fan, Z. Lan, S. Yin, T. Sato, Adv. Mater. 24 (2012) 1884.
[33] M. Grätzel, Prog. Photovolt. Res. Applic. 8 (2000) 171.
[34] G. Wang, W. Xing, S. Zhuo, Electrochim. Acta 66 (2011) 151.
[35] S. Patil, P. Deshmukh, C. Lokhande, Sensors Actuat B 156 (2011) 450.
[36] S. Ameen, M. Akhtar, Y. Kim, O. Yang, H. Shin, J. Phys. Chem. C 114 (2010) 4760.
[37] Y. Lin, D. Li, J. Hu, G. Xiao, J. Wang, W. Li, X. Fu, J. Phys. Chem. C 116 (2012) 5764.
[38] D. Bi, S. Moon, L. Häggman, G. Boschloo, L. Yang, E. Johansson, M. Nazeeruddin, M. Grätzel, A. Hagfeldt, RSC Adv. 3 (2013) 18762.
[39] H. Lin, C. Huang, W. Li, C. Ni, S. Shah, Y. Tseng, Appl. Catal. B-Environ 68 (2006) 1.
[40] H. Kim, C. Lee, J. Im, K. Lee, T. Moehl, A. Marchioro, S. Moon, R. Humphry-Baker, J. Yum, J. Moser, M. Grätzel, N. Park, Sci. Rep. 2 (2012) 591.
[41] Y. Zhao, J. Zhai, T. Wei, L. Jiang, D. Zhu, J. Mater. Chem. 17 (2007) 5084.
[42] Y. Zhao, J. Zhai, J. He, X. Chen, L. Chen, L. Zhang, Y. Tian, L. Jiang, D. Zhu, Chem. Mater. 20 (2008) 6022.
[43] H. Kim, J. Lee, N. Yantara, P. Boix, S. Kulkarni, S. Mhaisalkar, M. Grätzel, N. Park, Nano Lett. 13 (2013) 2412.
[44] W. Li, J. Li, L. Wang, G. Niu, R. Gao, Y. Qiu, J. Mater. Chem. A 1 (2013) 11735.
[45] G. Niu, W. Li, F. Meng, L. Wang, H. Dong, Y. Qiu, J. Mater. Chem. A 2 (2014) 705.
[46] L. Heng, X. Wang, N. Yang, J. Zhai, M. Wan, L. Jiang, Adv. Funct. Mater. 20 (2010) 266.
[47] S. Ito, Y. Makri, J. Kitamura, J. Mater. Chem. 14 (2004) 385.
[48] G. Mor, K. Shankar, M. Paulose, O. Varghese, C. Grimes, Nano Lett. 6 (2006) 215.
[49] E. Ramasamy, W. Lee, D. Lee, J. Song, J. Power Sources 165 (2007) 446.